Journal of Magnetic Resonance **156,** 187–194 (2002)
doi:10.1006/jmre.2002.2549

Tagging of the Magnetization with the *Transition Zones* of 360° Rotations Generated by a Tandem of Two Adiabatic DANTE Inversion Sequences

Nikolaos V. Tsekos,*[,1] Michael Garwood,† and Kâmil Ugurbil†

*Cardiovascular Imaging Laboratory, Mallinckrodt Institute of Radiology, Washington University Medical Center, 510 S. Kingshighway Blvd., Box 8225, St. Louis, Missouri 63110; and †Center for Magnetic Resonance Research and Department of Radiology, University of Minnesota, 2021 6th Street SE, Minneapolis, Minnesota 55455

Received July 9, 2001; revised March 30, 2002

A new technique is presented for generating myocardial tagging using the signal intensity minima of the transition zones between the bands of 0° and 360° rotations, induced by a tandem of two adiabatic delays alternating with nutations for tailored excitation (DANTE) inversion sequences. With this approach, the underlying matrix corresponds to magnetization that has experienced 0° or 360° rotations. The DANTE sequences were implemented from adiabatic parent pulses for insensitivity of the underlying matrix to B_1 inhomogeneity. The performance of the proposed tagging technique is demonstrated theoretically with computer simulations and experimentally on phantom and on the canine heart, using a surface coil for both RF transmission and signal reception. The simulations and the experimental data demonstrated uniform grid contrast and sharp tagging profiles over a twofold variation of the B_1 field magnitude.

Key Words: **tagging; adiabatic pulses; heart; canines.**

INTRODUCTION

The mechanical function of the heart can be rigorously and noninvasively evaluated with myocardial tagging techniques (*1–3*). Myocardial tagging has evolved to a robust tool for the study of heart wall motion on humans and animal models (e.g., (*4–16*)). With myocardial tagging, a grid is generated on the heart by modulating the longitudinal magnetization (M_z) with a series of low signal intensity bands using trains of RF pulses together with pulsed B_0 gradients. The tagging grid can be generated with direct modulation of M_z using trains of band-selective RF pulses (*1, 17, 18*) or multiband delays alternating with nutations for tailored excitation (DANTE) pulse sequences (*4, 19*). Alternatively, the transverse magnetization (M_{xy}) can be modulated with B_0 gradients with the spatial modulation of magnetization (SPAMM) sequence (*2, 3, 20*), before it is restored on the longitudinal axis.

Several technical advances of the tagging techniques have been introduced for improved and tailored tagging grids. As an example, the frequency profile of the tagging bands generated by the SPAMM technique can be refined by using trains of nonselective pulses with their relative amplitudes modulated by binomial coefficients (*3*). For improved density and bandwidth of tagging, the B_0 gradient waveform of SPAMM or DANTE sequences can be modulated with a saw-tooth-like pattern (*18*). Adiabatic SPAMM (*9*) or DANTE (*21*) sequences have been shown to produce constant grid width and contrast as required when transmitting RF with the highly inhomogeneous B_1 produced with a surface coil. Approaches have also been introduced for improved tag contrast reducing the signal loss due to T_1 relaxation (*22*) and to account for through-plane motion (*23*). Recently, a method was demonstrated for variable tagging spacing defined interactively by the user for improved coverage of the heart, using concepts from the k-space excitation theory (*24*).

Myocardial tagging can provide a plethora of information, otherwise unavailable, about the cardiac contractile apparatus such as transmyocardial point displacement and global and regional myocardial strain (e.g., (*20, 25–28*)). In view of the robustness of myocardial tagging methods, it is possible to foresee their combination with other MR techniques for the integrated study of cardiac physiology. Integrating MR techniques may provide new insight into heart pathophysiology in animal models and, eventually, in humans. Such an approach is further supported by a growing body of literature in cardiac physiology which suggests that such integrated implementation may be necessary since no single physiological index is suitable to adequately characterize the complex cardiac pathophysiology (*29, 30*). Recently, myocardial tagging has been combined with perfusion contrast (*11*) and localized ^{31}P spectroscopy (*31*). At high spatial resolution (*32, 33*), it is often desirable to generate tags with narrow grid width and minimal unwanted modulation of the underlying matrix. Such features can be beneficial for high resolution studies of the myocardium, particularly in small animal models. One approach to generating a tagging grid with narrow stripes uses the signal intensity (SI) minima in the frequency response profile where M_z crosses through zero (i.e., the transition zones between the inverted and uninverted bands of magnetization). In magnitude images, these transition zones correspond to a signal of reduced intensity relative to the underlying matrix.

[1] To whom correspondence should be addressed.

1090-7807/02 $35.00

Myocardial tagging using the zero crossings of M_z was first demonstrated by Axel and Dougherty (*3*) using a 90°–G_i–90° SPAMM sequence, where G_i is a gradient pulse along direction i (=x, y, or z). Although a 90°–G_i–90° SPAMM or, equivalently, a DANTE inversion sequence can generate a narrow tagging grid, the underlying matrix is composed of alternating bands of $+M_z$ and $-M_z$. As a consequence, the tagging grid spacing and the matrix contrast are affected by B_1 inhomogeneity and T_1 relaxation (*3*). In this report, we present a myocardial tagging technique using a tandem of two adiabatic DANTE inversion sequences, which obviates the above limitations and generates a fine tagging grid. This technique is demonstrated on phantom and animal studies using surface coils for RF transmission and reception.

MATERIAL AND METHODS

Tagging with the Intensity Minima of the Transition Zones of RF Pulses

Figure 1 illustrates the proposed technique for generation of a tagging grid using the signal intensity minima of DANTE inversion sequences at the offset frequencies where the M_z crosses through zero. This technique uses a tandem of two DANTE inversion pulse sequences, P_1 and P_2, applied in the presence of appropriate B_0 selection gradients, S_1 and S_2, as shown in Fig. 1A. Additional B_0 gradients, C_1 and C_2, can be interleaved with the two pulses to dephase unwanted M_{xy}. For generation of a two-dimensional rectangular grid, the above sequence can be repeated with the selection gradients S_1 and S_2 applied on an orthogonal direction.

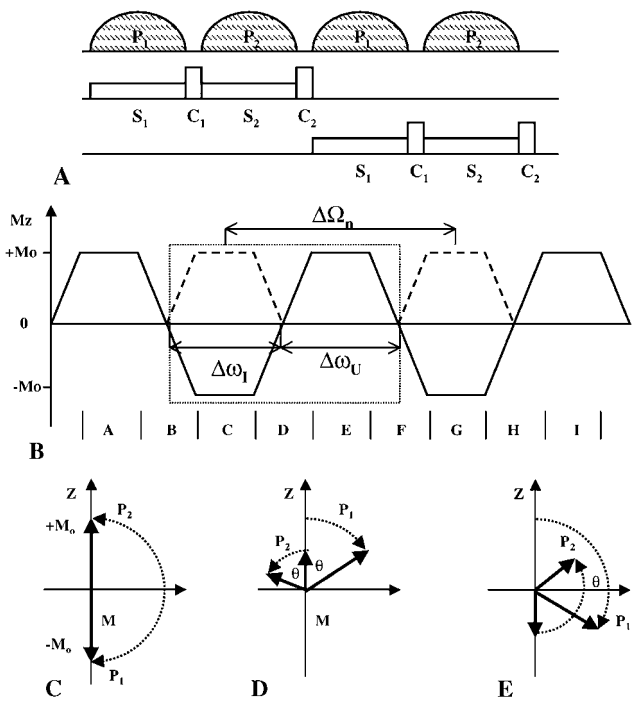

FIG. 1. The proposed technique, illustrating the timing diagram of the RF pulse sequence (A), a diagrammatic representation of the frequency response of the adiabatic pulses (B), and illustrations of the magnetization for (C) 180°, (D) $0° < \theta < 90°$, and (E) $90° < \theta < 180°$ rotations. P_1 and P_2 are adiabatic DANTE inversion pulse sequences, S_1 and S_2 are selective B_0 gradients, and C_1 and C_2 are B_0 gradients to dephase M_{xy}. The frequency profile (B) depicts a representation of the frequency profile of a single adiabatic DANTE pulse sequence (solid line) and of a tandem (dashed). The dotted box represents the periodic element of the tagging profile. This graphical representation does not depict the exact profile of the transition zone.

A DANTE inversion sequence generates a periodic modulation of M_z which is composed of bands with unperturbed ($M_z = +M_0$; zones A, E, and I) and inverted magnetization ($M_z = -M_0$; zones C and G), as illustrated in Fig. 1B. The frequency separation $\Delta\Omega_n$ (peak-to-peak) of the inverted bands depends on the interpulse delay and the applied selection gradient, while the width of the inverted bands $\Delta\omega_I$ (zero-crossing points) depends on the total duration of the applied DANTE sequence (*2, 19, 21*). The unperturbed and inverted bands are interleaved with *transition zones*, in which the magnetization has experienced a range of rotation angles, θ, with $0° < \theta < 180°$ ($-M_0 < M_z < +M_0$; zones B, D, F, and H). After dephasing M_{xy} with the B_0 gradient pulse, C_1, the M_z in the transition zones is equal to $M_0\cos(\theta)$ and it crosses through the zero twice within a periodic element of the frequency profile (as, for example, delineated with the dotted box in Fig. 1B). Specifically, the magnetization crosses through zero at intervals $\Delta\omega_I$ and $\Delta\omega_U$; the latter is the nominal width of the unperturbed band. Thus, in a magnitude image collected immediately after the pulse P_1, the zero crossing points will correspond to signal intensity minima and they can be used to generate a tagging grid. However, T_1 relaxation will alter the contrast of the tissue in the alternating inverted bands of the tagging matrix and in the transition zones defining the tagging grid. In practice, alternating bands of inverted magnetization in the tagging matrix will demonstrate an undesired time dependent contrast, particularly as $M_z(t)$ passes through zero, in a similar manner to that reported by Axel *et al.* (*3*). This can be minimized with the application of a second inversion pulse, P_2, immediately after the first one (P_1) to restore the magnetization of the inverted bands and the transition zones along the $+z$ axis. Therefore, the M_z of the underlying matrix will experience T_1 relaxation starting from a positive value, alleviating the previously described undesired contrast time evolution when it would have started from a negative value.

Specifically, a pulse P_2, identical to P_1 applied with the same selection gradients S_1 and S_2, will induce the same inversion profile on the underlying matrix. The pulse P_2 can be applied with a 180° phase compared to the P_1 to remove imperfections in the pulse performance. Following the pulse P_2, the magnetization of the noninverted bands (A, E, and I) will remain relatively unaffected. However, the magnetization of the inverted bands (C and G) will rotate by $-180°$ and will rest along the $+z$ axis (dashed line in Fig. 1B). The transition zones (B, D, F, and H) will experience a $-\theta$ rotation and, therefore, following a second

B_0 spoiler gradient, S_2, M_z will be proportional to $M_0\cos^2(\theta)$. In particular, assuming perfect dephasing by the gradient C_1, the magnetization at the zero crossing points, where $\theta = 90^\circ$, will remain dephased and with $M_z = 0$. As a consequence, the underlying matrix that corresponds to the bands A, C, E, G, and I will have M_z along the $+z$ axis and the tagging grid will be defined by the SI minima of the transition zones (B, D, F, and H), as depicted with the dashed lines in Fig. 1B. Moreover, the dual-pulse sequence produces sharper boundaries, due to the quadrature dependence of the M_z modulation, i.e., $M_0\cos^2(\theta)$, when compared to the single-pulse tagging sequence that generates a first-order modulation of the M_z, i.e., $M_0\cos(\theta)$. The diagrams in Figs. 1C, 1D, and 1E illustrate the rotations of the magnetization that experiences 180°, $0^\circ < \theta < 90^\circ$, and $90^\circ < \theta < 180^\circ$, respectively.

Tagging with the proposed technique is based on the flexibility of the DANTE sequences to define a desired inversion profile, i.e., the parameters $\Delta\Omega_n$, $\Delta\omega_I$, and $\Delta\omega_U$, with appropriate manipulation of the DANTE segmentation and choice of the parent pulse. Specifically, for generation of a tagging pattern with uniform spacing, it is required that the nominal bandwidth of the inversion band, $\Delta\omega_I$, be equal to the bandwidth of the undisturbed bands, $\Delta\omega_U$, i.e., $\Delta\omega_I = \Delta\omega_U$, since both bands correspond to a nontagged matrix. Consequently, the peak-to-peak spectral spacing of the inverted bands ($\Delta\Omega_n$) should be twice the inversion bandwidth ($\Delta\omega_I$):

$$\Delta\Omega_n = 2\Delta\omega_I = 2\Delta\omega_U. \quad [1]$$

This requirement is different from the case in which the tagging grid is generated by the inversion or saturation bands of a DANTE sequence (*4*). In this case, the width of the inverted or saturated band is less than the width of the underlying matrix; i.e., $\Delta\omega_I < \Delta\omega_U$.

Axel and Dougherty (*3*) first described tagging with magnetization zero-crossings in the SPAMM method. With SPAMM, a high density tagging grid is generated with a 90°–G–90° sequence, which creates a sinusoidal modulation of the M_z. The tagging grid is then created by dephasing M_{xy} in the intervening (transition) bands in a similar manner to that described above. However, as it was demonstrated experimentally by Axel and Dougherty (*3*), the grid generated by a 90°–G–90° SPAMM is affected by T_1 relaxation and B_1 inhomogeneity. Specifically, after the second 90° pulse, the magnetization in alternating bands is inverted and undergoes T_1 relaxation, resulting in progressively reduced signal intensity of the corresponding bands of the matrix. Furthermore, for delays shorter than T_1 ln(2), the width of bands converges. B_1 inhomogeneity will have a similar effect on the tagging grid contrast and spacing. Such inhomogeneity will generate a nonuniform spatial distribution of M_z after the tagging pulses; subsequent T_1 relaxation will further amplify the nonuniformity of the underlying matrix. Similar effects on the contrast of the underlying matrix and the tagging grid occur when a single DANTE inversion is used.

In the proposed technique, implementing a tandem of two adiabatic DANTE inversion pulse sequences minimizes the aforementioned limitations. First, by using a tandem of inversions, the underlying matrix corresponds to noninverted magnetization ($+M_z$), and thus, unwanted contrast modulation due to T_1 relaxation is minimal (considering that T_1 decay is minimal during the application of the pulses). Second, sensitivity to B_1 inhomogeneity is reduced with adiabatic pulses, which makes the technique advantageous for use with surface coils.

Implementation with Adiabatic DANTE Inversion Sequences

An adiabatic DANTE pulse sequence is generated by segmenting the amplitude ($B_1(t)$) and the frequency or phase ($\Phi(t)$) modulation functions of an adiabatic full-passage pulse (the parent pulse) into N elements, each of length ΔT_p, and inserting delay periods, τ, between the elements as described in (*21, 34*), and graphically depicted in the graphs of Figs. 2A

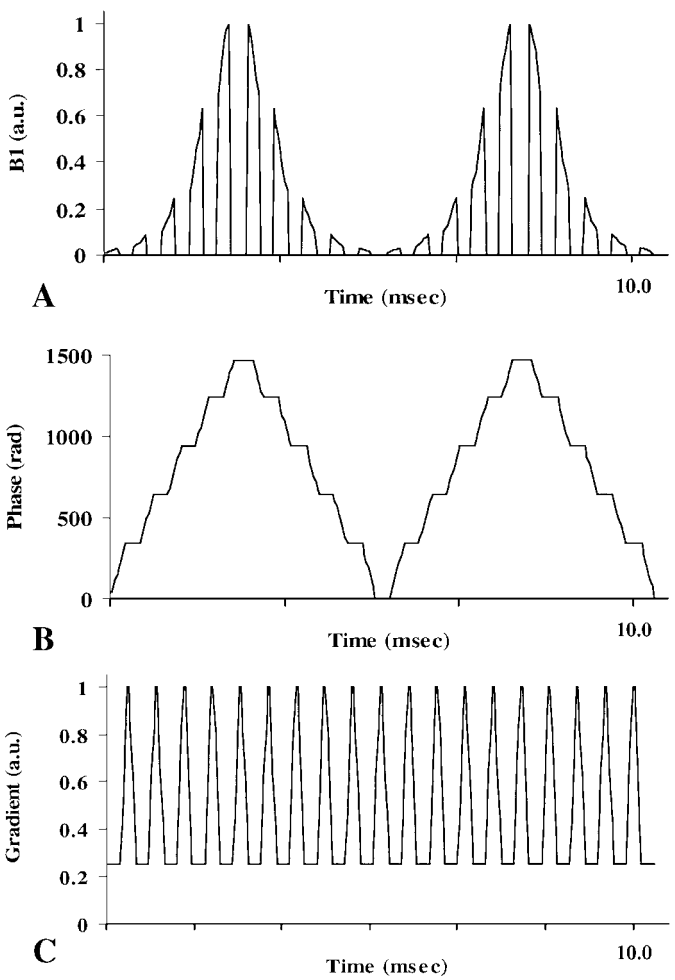

FIG. 2. The amplitude, $B_1(t)$ (A), and phase, $\Phi(t)$ (B), modulation functions of the tandem of two adiabatic DANTE inversion sequences based on hyperbolic secant parent pulses and the corresponding gradient waveform (C). These adiabatic DANTE inversion profiles were generated with $R = 8.04$, $\alpha = 2$, and $\varepsilon = 3$.

and 2B. The resulting DANTE sequence retains the insensitivity of the parent pulse to B_1 inhomogeneity. The inversion bandwidth is $\Delta\omega_{\max} T_p/\pi T_{\text{tot}}$, where $\Delta\omega_{\max}$ is the amplitude of the frequency modulation (in rad/s) and T_p is the duration of the parent pulse (in s). Following the standard nomenclature, the parameter $R = \Delta\omega_{\max} T_p/\pi$ can be used to characterize both the parent and the DANTE adiabatic pulses (*35*). Figure 2 illustrates an example of a tandem of adiabatic DANTE pulse sequences generated by using hyperbolic secant (*36*) modulation functions with $R = 8.04$.

For the generation of a tagging grid, B_0 gradients are used for spatial encoding of the frequency response (*19*). It has been demonstrated that the saw-tooth-like gradient waveform shown in Fig. 2C better suits the case of adiabatic pulses (*21*). This gradient waveform consists of a constant base gradient (G_B), during the application of the DANTE pulse elements, which is ramped up to a maximum ($G_B + G_M$) and down to the base (G_B) during each τ delay (Fig. 2C). This gradient waveform allows the generation of a dense tagging grid without requiring an increase of the pulse duration or the strength of the dispersion gradient; the latter results in an undesired reduction of the tagged matrix area (*18, 21*). By defining $\alpha = \tau/\Delta T_p$ and $\varepsilon = G_M/G_B$, it can be shown that the ratio of the tagging grid distance (L) and the grid width (l), is given by (*21*):

$$\frac{\Delta\Omega_n}{\Delta\omega_I} = \frac{\Delta\omega_I + \Delta\omega_U}{\Delta\omega_I} = \frac{L}{l} = \frac{(N-1)(1+\alpha+0.5\varepsilon\alpha)+1}{R\pi(1+\alpha+0.5\varepsilon\alpha)}. \quad [2]$$

The requirement for uniform spacing of the tagging grid, Eq. [1], determines the relationship of the parameters of the DANTE sequence R, N, α, and τ.

$$R = \frac{N-1}{2\pi} + \frac{1}{2\pi(1+\alpha+0.5\varepsilon\alpha)} \quad [3]$$

In principle, an unlimited number of sets of parameters R, N, α, and τ can be chosen to satisfy the above equation. In practice several limitations may be imposed on these choices, such as the available peak RF power, the maximum gradients strength and slew rate, and the satisfaction of the adiabatic condition. For example, imperfections in pulse performance reduce as the value of R increases (*35*), but only at the expense of requiring higher peak RF power or longer duration (T_{tot}). High pulse duration is not desirable for working with the heart, due to motion, and in addition it may result in unwanted T_1 decay. Practically, one may first decide on the segmentation of the parent pulse considering the available B_0 gradients and RF power, i.e., choice of N, α, and τ. Then the R value can be easily adjusted to satisfy the requirements of Eqs. [1] and [2]. Noticeably, all the involved parameters, except N, can be nonintegers, which facilitates the unconstrained design of the DANTE sequences.

Figure 3 illustrates the response of M_z to a single adiabatic inversion DANTE sequence (A and C) and to a tandem of two identical inversions (B and D). Figures 3A and 3B show the performance of the single and the tandem, respectively, as a function of offset frequency for $\gamma B_1/2\pi = 2.5$ kHz. When a single adiabatic DANTE is applied, the magnetization is modulated with inversion bands that have the same bandwidth (at zero-crossing) as that of the unaffected matrix (Fig. 3A). When the tandem DANTE is applied, the longitudinal magnetization M_z is modulated with narrow tagging lines (Fig. 3B). Noticeably, the outermost bands of the frequency profile demonstrate minor imperfections that may be caused by the off-resonance performance of the DANTE sequence. Figures 3C and 3D show the B_1 response of the single and the tandem DANTE pulses, demonstrating high tolerance to large increases of the B_1 above a threshold. Some minor oscillations of the magnetization are observed in Fig. 3D at higher B_1 that result from the use of a relatively low R value (*21*). Both the imperfection in the outer bands of the frequency response (Fig. 3B) and the oscillations of the B_1 response (Fig. 3D) will have negligible effect on the tagged images.

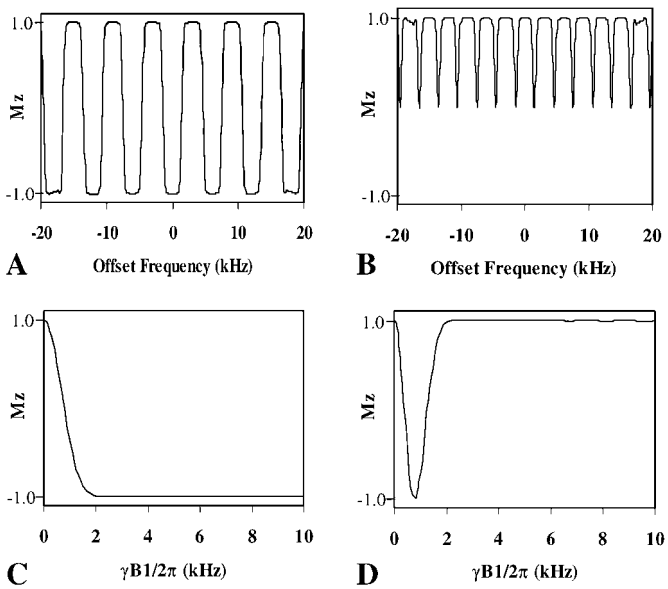

FIG. 3. The calculated M_z following a single adiabatic DANTE inversion (A and C) and a tandem of two identical adiabatic DANTE inversions (B and D) as a function of frequency offset (A and B) and B_1 (C and D). The profiles were produced with the adiabatic pulse sequences depicted in Fig. 2. The frequency profiles (A and B) were calculated with $\gamma B_1/\pi = 2.5$ kHz and the B_1 response at zero offset.

MR Imaging Protocol

All experiments were conducted on a 4.7 T/40 cm horizontal bore magnet interfaced to a Varian $^{\text{Unity}}$INOVA console, using a linear dual loop surface coil (each loop diameter = 13 cm) for both transmission and signal reception. A magnetization prepared segmented gradient recalled echo (GRE) sequence was used for imaging, with the tagging pulses applied before the acquisition of each k-space segment. Phantom studies (TR/TE/flip

angle = 6.8 ms/4.5 ms/11°, 256 × 256, FOV = 12 × 12 cm, 8 segments) were conducted on a 10-cm plastic flask filled with 125-mM P_i in water. *In vivo* demonstration was performed on a closed-chest canine model ($n = 3$), with a heparin-filled catheter introduced in the left ventricular (LV) cavity to provide a triggering signal. To minimize motion artifacts, both the cardiac and respiratory cycles were synchronized with data acquisition. The heart rate was typically in the range of 120–140 bpm and the tagging pulse was applied in mid-diastole. Following the triggering signal, the GRE sequence (TR/TE/flip angle = 5.1 ms/2.7 ms/22°, 256 × 128, FOV = 12 × 12 cm^2) was acquired in eight consecutive segments and cardiac multiphase images were collected by incrementing the delay between the tagging pulses and the imaging sequence, as described elsewhere (*21*). The DANTE inversion sequence was generated from a hyperbolic secant parent pulse with $R = 8.04$ ($N = 17$, $\Delta T_p = 204$ μs, $\tau = 408$ μs, $\alpha = 2$, $T_{tot} = 10$ ms). Long pulse duration (the duration of the parent pulse was 3.47 ms) and small α were chosen due to limited RF power. The gradient waveform was applied with base gradient $G_B = 0.2$ G/cm and maximum $G_B + G_M = 0.9$ G/cm.

RESULTS AND DISCUSSION

Figure 4 demonstrates the effect of increased RF power on the performance of the adiabatic DANTE tandem pulses on the phantom. In these studies, the image plane was set parallel to the surface coil so that the B_1 gradient was minimal (~2-fold). The effect of changing B_1 amplitude was investigated by varying the transmitter power from 100 to 900 W resulting in a B_1 range of 0.9 to 2.8 kHz at the center of the coil. At low power levels, magnetization was not inverted by the first pulse, and after the second pulse, the final magnetization was considerably less than M_0. This caused a significant reduction in signal intensity in alternating bands (images A and B). With a further increase of power (image C), the initial pulse began to invert magnetization and the signal reappeared in these alternating bands as the second pulse rotated a portion of $-M_z$ back to the $+z$ axis. As the RF power increased in images C to F, the tandem of pulses gradually became fully adiabatic, and matrix contrast became uniform, first at the center of the coil where B_1 was highest (image C), and then progressively outward to the edges of the coil (images D to F). In agreement with simulations, these experiments demonstrate an ability to produce a sharp tagging grid that remains unchanged despite increasing B_1 above a threshold level.

Tagged images with the proposed method were collected on three canines and we demonstrated the generation of a sharply defined tagging grid with uniform contrast despite B_1 inhomogeneities due to the use of surface RF coil. Figure 5 illustrates the performance of the tagging grid generated by the proposed method on a canine heart. The panel of images in Fig. 5 illustrates nine views of the heart at different phases of a complete cardiac cycle. Each segment was collected with 40-ms temporal

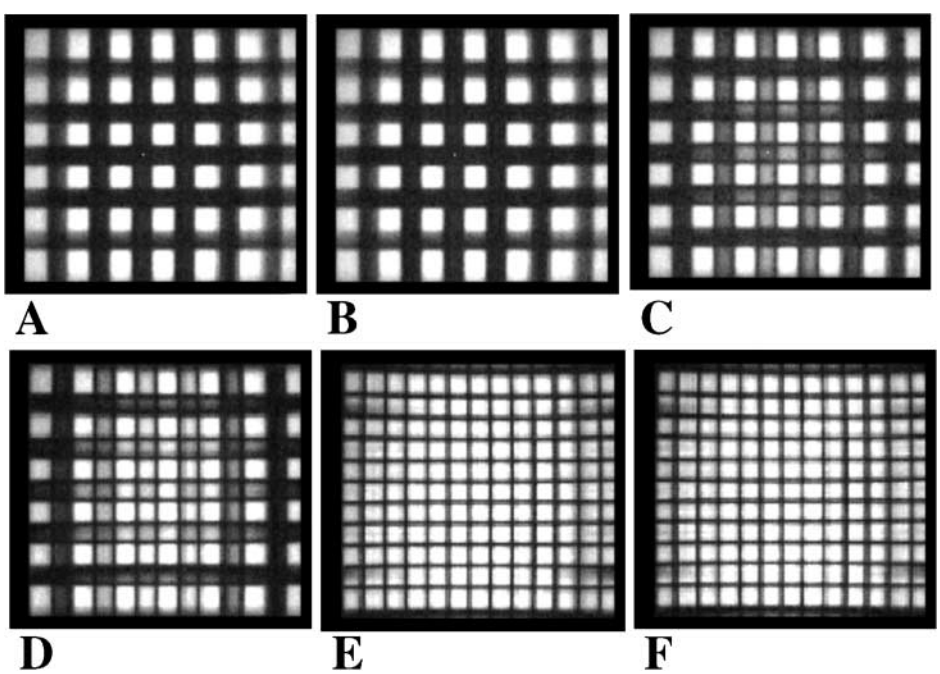

FIG. 4. A series of tagged phantom images in a coronal plane, generated with the tandem adiabatic DANTE sequences, using RF power of 100 (A), 200 (B), 300 (C), 500 (D), 700 (E), and 900 W (F). The B_1 at the center of the coil was approximately 0.9 (A), 1.3 (B), 1.6 (C), 2.1 (D), 2.5 (E), and 2.8 kHz/2π (F). Since the coronal plane is parallel to the surface coil, the underlying matrix contrast alterations are due to the power changes. This panel of images demonstrates the principle of tagging with the transition zones of 360° rotations. The grid width is 3.8 × 3.8 mm.

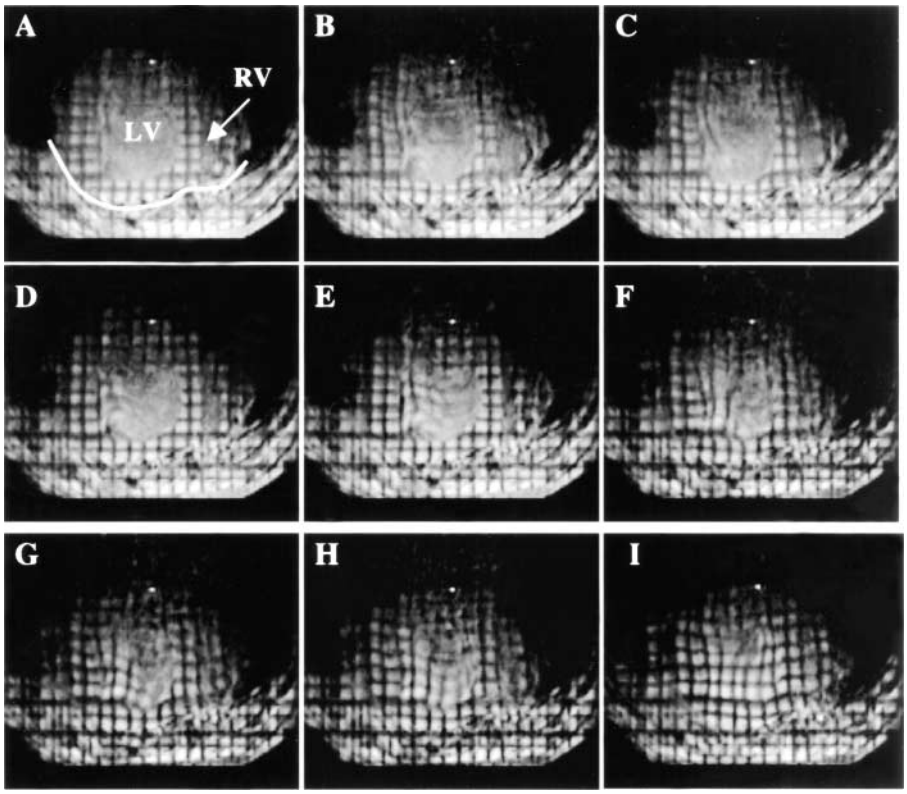

FIG. 5. Short apical-view images of tagged canine heart at 4.7 T, using the tandem of two adiabatic DANTE inversion sequences, showing nine phases of a cardiac cycle. The white line outlines the heart relative to the chest wall (LV, left ventricle; RV, right ventricle). Images (A) to (F) correspond to diastole and images (G) to (I) to systole. The delay between the tagging pulse and the acquisition of each image was incremented every 40 ms and the transmitter power was 900 W. The imaging plane is perpendicular to the surface coil plane. The tagging pulse was generated from a hyperbolic secant parent pulse with $R = 8.04$, $N = 17$, $\Delta T_p = 204$ μs, $\tau = 408$ μs, $\alpha = 2$, and $T_{\text{tot}} = 10$ ms.

resolution and the heart rate was 140 bpm. The diastolic dimensions of the tagging grid were 3.8×3.8 mm^2. The tagging grid translational and rotational deformation, due to apex motion, is clearly depicted especially during systole (images G to I) while it remained undistorted at the end diastolic phase (A). The tagging grid was sharply defined, as expected from the concept of the proposed tagging method and the simulation results (Fig. 2). Although the imaged plane was perpendicular to the surface coil, resulting in a large B_1 gradient, the tagging grid and the underlying tissue matrix demonstrate uniform contrast that is retained at later heart phases. Noticeably, some blurring of the tagging grid and the heart is observed, most probably attributed to the particular way we acquired the segmented images. Since each segment was individually collected after a trigger signal every fourth heartbeat, the images were prone to motion artifacts, for example due to imperfect synchronization of the cardiac and respiratory cycles. This blurring, which was also observed at other tagged series, was due to the used pulse sequence and is not related to the tagging technique as it may have appreciated from the tagged images of the stationary phantom in Fig. 4.

Tagging with the transition zones of a pulse is, conceptually, a unique idea, first introduced by Axel and Dougherty (*3*). In previously described MR tagging techniques, the grid is generated by the excitation or inversion band of the pulse, i.e., trains of band-selective pulses (*1*) or DANTE sequences (*19*), or by modulation of M_{xy} by a B_0 gradient (*3*). In many of these techniques, B_1 variations modulate the signal intensity and contrast the underlying tissue and the width of the alternating bands, as we have demonstrated previously (*21*). With the method presented here, the bands of the preparatory pulses leave the underlying matrix relatively unaffected and the tagging grid is generated by the SI minima of the transition zones between these bands.

The proposed technique generates a fine tagging grid, a property that is beneficial for animal studies with thin myocardium. However, it should be emphasized that high tagging grid resolution (small peak-to-peak distance and grid width) requires accordingly the presence of sufficient in-plane spatial resolution (*32, 33*). In addition, tagging with conventional pulses requires relatively large areas of homogeneous B_1 fields for generation of a tagging grid with uniform contrast relative to the underlying matrix. Although torso-circumscribing coils provide sufficient B_1 homogeneity, the use of such coils for small bore animal magnets is not always feasible due to bore size limitations. RF

transmission (and reception) with a surface is one solution to this problem, and the implementation of an adiabatic method such as that described here ensures that the tagging grid width and contrast are insensitive to changes in B_1. An additional benefit of using adiabatic pulses is the fact that the tailoring of the frequency profile spacing, i.e., l and L, is straightforward by adjusting the R-value, as dictated by Eqs. [2] and [3]. Such adjustments do not affect the tagging grid magnetization profile since the shape of the pulse is not changing. Using adiabatic pulses with different modulation functions, such as those based on offset-independent adiabaticity (*37, 38*), represents yet another possibility for varying the grid width (l) and for reducing peak RF power requirements.

CONCLUSION

A method to generate a tagging grid using the transition zones of 360° rotations induced by a tandem of two adiabatic inversion DANTE sequences has been described. Theoretical simulations and experimental studies on phantoms and canines demonstrated that this approach can generate a sharp tagging grid, which is insensitive to B_1 inhomogeneity, appropriate for high resolution assessment of myocardial wall motion.

ACKNOWLEDGMENTS

This work was supported by a Biomedical Engineering Grant from The Whitaker Foundation (NVT), and NIH Grants P41RR08079 and HL 33600.

REFERENCES

1. E. A. Zerhouni, D. M. Parish, W. J. Rogers, A. Yang, and E. S. Shapiro, Human heart: tagging with MR imaging—A method for noninvasive assessment of myocardial motion, *Radiology* **169,** 59–63 (1988).
2. L. Axel and L. Dougherty, Heart wall motion: Improved method of spatial modulation of magnetization for MR imaging, *Radiology* **172,** 349–350 (1989).
3. L. Axel and L. Dougherty, MR imaging of motion with spatial modulation of magnetization, *Radiology* **171,** 841–845 (1989).
4. A. J. de Crespigny, T. A. Carpenter, and L. D. Hall, Cardiac tagging in the rat using a DANTE sequence, *Magn. Reson. Med.* **21,** 151–156 (1991).
5. E. R. McVeigh and E. A. Zerhouni, Noninvasive measurement of transmural gradients in myocardial strain with MR imaging, *Radiology* **180,** 677–683 (1991).
6. S. E. Maier, S. E. Fischer, G. C. McKinnon, O. M. Hess, H. P. Krayenbuehl, and P. Boesiger, Evaluation of left ventricular segmental wall motion in hypertrophic cardiomyopathy with myocardial tagging. *Circulation* **86,** 1919–1928 (1992).
7. Z. A. Fayad, D. L. Kraitchman, V. A. Ferrari, and L. Axel, Right ventricular regional function in normal subjects using magnetic resonance tissue tagging, *in* "2nd Meeting of the Society of Magnetic Resonance, San Francisco, CA, 1994."
8. C. M. Kramer, N. Reichek, V. A. Ferrari, T. Theobald, J. Dawson, and L. Axel, Regional heterogeneity of function in hypertrophic cardiomyopathy, *Circulation* **90,** 186–194 (1994).
9. K. Hendrich, Y. Xu, S. G. Kim, and K. Ugurbil, Surface coil cardiac tagging and 31P spectroscopic localization with B1-insensitive adiabatic pulses, *Magn. Reson. Med.* **31,** 541–545 (1994).
10. J. A. Lima, V. A. Ferrari, N. Reichek, C. M. Kramer, L. Palmon, M. R. Llaneras, B. Tallant, A. A. Young, and L. Axel, Segmental motion and deformation of transmurally infarcted myocardium in acute postinfarct period, *Am. J. Physiol.* **268,** H1304–1312 (1995).
11. D. L. Kraitchman, N. Wilke, E. Hexeberg, M. Jerosch-Herold, Y. Wang, T. B. Parrish, C. N. Chang, Y. Zhang, R. J. Bache, and L. Axel, Myocardial perfusion and function in dogs with moderate coronary stenosis, *Magn. Reson. Med.* **35,** 771–780 (1996).
12. C. Matter, E. Nagel, M. Stuber, P. Boesiger, and O. M. Hess, Assessment of systolic and diastolic LV function by MR myocardial tagging, *Basic Res. Cardiol.* **91,** 23–28 (1996).
13. J. T. Marcus, M. J. Gotte, A. C. Van Rossum, J. P. Kuijer, R. M. Heethaar, L. Axel, and C. A. Visser, Myocardial function in infarcted and remote regions early after infarction in man: assessment by magnetic resonance tagging and strain analysis, *Magn. Reson. Med.* **38,** 803–810 (1997).
14. J. A. Lima, R. Jeremy, W. Guier, S. Bouton, E. A. Zerhouni, E. McVeigh, M. B. Buchalter, M. L. Weisfeldt, E. P. Shapiro, and J. L. Weiss, Accurate systolic wall thickening by nuclear magnetic resonance imaging with tissue tagging: correlation with sonomicrometers in normal and ischemic myocardium, *J. Am. Coll. Cardiol.* **21,** 1741–1751 (1993).
15. E. R. McVeigh, F. W. Prinzen, B. T. Wyman, J. E. Tsitlik, H. R. Halperin, and W. C. Hunter, Imaging asynchronous mechanical activation of the paced heart with tagged MRI, *Magn. Reson. Med.* **39,** 507–513 (1998).
16. Z. A. Fayad, V. A. Ferrari, D. L. Kraitchman, A. A. Young, H. I. Palevsky, D. C. Bloomgarden, and L. Axel, Right ventricular regional function using MR tagging: normals versus chronic pulmonary hypertension, *Magn. Reson. Med.* **39,** 116–123 (1998).
17. B. D. Bolster, E. R. McVeigh, and E. A. Zerhouni, Myocardial tagging in polar coordinates with use of striped tags, *Radiology* **177,** 769–772 (1990).
18. E. R. McVeigh and E. Atalar, Cardiac tagging with breath-hold cine MRI, *Magn. Reson. Med.* **28,** 318–327 (1992).
19. T. J. Mosher and M. B. Smith, A DANTE tagging sequence for the evaluation of translational sample motion, *Magn. Reson. Med.* **15,** 334–339 (1990).
20. A. A. Young and L. Axel, Three-dimentional motion and deformation of the heart wall: Estimation with spatial modulation of magnetization—A model-based approach, *Radiology* **185,** 241–247 (1992).
21. N. V. Tsekos, M. Garwood, H. Merkle, Y. Xu, N. Wilke, and K. Ugurbil, Myocardial tagging with B1 insensitive adiabatic DANTE inversion sequences, *Magn. Reson. Med.* **34,** 395–401 (1995).
22. S. E. Fischer, G. C. McKinnon, S. E. Maier, and P. Boesiger, Improved myocardial tagging contrast, *Magn. Reson. Med.* **30,** 191–200 (1993).
23. S. E. Fischer, G. C. McKinnon, M. B. Scheidegger, W. Prins, D. Meier, and P. Boesiger, True myocardial motion tracking, *Magn. Reson. Med.* **31,** 401–413 (1994).
24. E. R. McVeigh and B. D. Bolster, Jr., Improved sampling of myocardial motion with variable separation tagging, *Magn. Reson. Med.* **39,** 657–661 (1998).
25. N. R. Clark, N. Reichek, P. Bergey, E. A. Hoffman, D. Brownson, L. Palmon, and L. Axel, Circumferential myocardial shortening in the normal human left ventricle: Assessment by magnetic resonance imaging using spatial modulation of magnetization, *Circulation* **84,** 67–74 (1991).
26. E. R. McVeigh and E. A. Zerhouni, Noninvasive measurement of transmural gradients in myocardial strain with MR imaging, *Radiology* **180,** 677–683 (1991).
27. A. A. Young, L. Axel, L. Dougherty, D. K. Bogen, and C. S. Parenteau, Validation of tagging with MR imaging to estimate material deformation, *Radiology* **188,** 101–108 (1993).

28. M. J. Moulton, L. L. Creswell, S. W. Downing, R. L. Actis, B. A. Szabo, M. W. Vannier, and M. K. Pasque, Spline surface interpolation for calculating 3-D ventricular strains from MRI tissue tagging, *Am. J. Physiol.* **270,** H281–297 (1996).

29. R. O. Bonow, Identification of viable myocardium, *Circulation* **94,** 2674–2680 (1996).

30. A. Kaul, There may be more to myocardial viability than meets the eye! *Circulation* **92,** 2790–2793 (1995).

31. N. V. Tsekos, H. Merkle, Y. Zhang, X. Hu, and K. Ugurbil, Anatomical correlation of high energy phosphate and wall motion during occlusion of a coronary artery on the closed-chest canine heart, *in* "Int. Soc. Magn. Reson. Med. Philadelphia, 1999."

32. E. Atalar and E. R. McVeigh, Optimum tag thickness for the measurement of motion by MRI, *in* "11th Annual Meeting, Society of Magnetic Resonance in Medicine, 1992."

33. E. R. McVeigh and L. Gao, Precision of tag position estimation in breath-hold CINE MRI: The effect of tag spacing, *in* "12th Annual Meeting, Society of Magnetic Resonance in Medicine, New York, NY, 1993."

34. Y. Ke, D. G. Schupp, and M. Garwood, Adiabatic DANTE sequences for B1-insensitive narrowband inversion, *J. Magn. Reson.* **96,** 663–669 (1992).

35. M. Garwood and K. Ugurbil, B1 insensitive adiabatic RF pulses, *NMR Basic Princ. Progr.* **26,** 110–147 (1992).

36. M. S. Silver, R. I. Joseph, and D. I. Hoult, Highly selective $\pi/2$ and π pulse generation, *J. Magn. Reson*. **59,** 347–351 (1984).

37. E. Kupce and R. Freeman, Optimized adiabatic pulses for wideband spin inversion, *J. Magn. Reson. A* **118,** 229–303 (1996).

38. A. Tannus and M. Garwood, Improved performance of frequency-swept pulses using offset-independent adiabaticity, *J. Magn. Reson. A* **120,** 133–137 (1996).